Microsystem Technologies (2024) 30:981–991
https://doi.org/10.1007/s00542-024-05643-w

TECHNICAL PAPER

Modeling and analysis of the effect of strain gradient to design diaphragm for pressure sensing application through finite element analysis

Prabhat Ranjan[1,2]

Received: 5 May 2023 / Accepted: 25 March 2024 / Published online: 16 April 2024

Abstract
Capacitive and optical-based pressure sensors are considered for wide application in industries and R&D labs due to their superior performance. In general, these sensors use a diaphragm as a sensing element that needs to be designed accurately to achieve the desired level of accuracy for a higher operating range of the sensor. To design such a diaphragm, the conventional strain-based model cannot be used efficiently as the strain gradient starts dominating to introduce non-linear deformation with respect to the applied load when the diaphragm thickness reduces or the operating range increases beyond a certain value. Thus, there is a need to establish a comprehensive understanding and accurate modeling method to establish the underlying mechanism of the strain gradient. In view of this, a finite element analysis is carried out with moving-mesh to investigate the effect of the strain gradient phenomenon extensively in this paper. For the investigation, a few parameters are studied such as strain, strain gradient, bending rigidity, and deflection. It shows that the strain gradient spreads radially on the diaphragm and its zone of influence depends on the thickness as well as the applied pressure. This increases the bending rigidity significantly and the diaphragm deflection becomes non-linear as compared to the classical theory of bending. For validation of the present model, the bending rigidity and the deflection behavior are also compared with an earlier developed mathematical model as well as experimental results, and the same is discussed in this paper. The present work is useful for an accurate design and optimization of a diaphragm or a flexure for small size or/and higher operating range of pressure sensors and actuators.

1 Introduction

In the present era of engineering, a wide range of pressure sensors and vacuum gauges are extensively being used for various fields to monitor and control any processes related to chemical engineering, semiconductor, micro-fabrication, biomedical, Petro-chemical, etc. (Li et al. 2022; Wang et al. 2022; Hu et al. 2022; Sanli et al. 2022).

To date, researchers have developed numerous techniques for pressure sensing applications. In general, capacitance type and optical type pressure sensors have gained more popularity due to their superior performance (Eswaran and Malarvizhi 2013; Jiang et al. 2017). The capacitive pressure sensor is widely used to measure pressure or vacuum in which force due pressure difference deflects the sensing diaphragm and the capacitance between the diaphragm and a fixed electrode changes (Lei et al. 2012; Chen and Mehregany 2008; Catling 1998). There are a few factors that have made the capacitive sensors popular such as simple structural design (Zhou et al. 2005), low-temperature sensitivity (Young et al. 2004; Lee and Wise 1982), radiation resistance (Gabrielson 1993), high sensitivity (He et al. 2018), and low response time (Wan et al. 2017). On other hand, Fabry–Perot Interferometer (FPI) based optical pressure sensors are also being widely explored (Kim and Neikirk 1995; Yin et al. 2014). The FPI sensors need to maintain an FPI cavity which consists of two mirror planes. One mirror plane of the cavity is a partially reflective surface of an optical fiber that is used to carry optical light and the other mirror plane is a full reflective diaphragm to respond to the applied pressure. The change in pressure leads to the change in the gap between these two planes which is detected based on

✉ Prabhat Ranjan
pranjan@barc.gov.in

[1] Homi Bhabha National Institute, Mumbai, India

[2] Bhabha Atomic Research Centre, Mumbai, India

the FPI technique to measure the pressure (Ghildiyal et al. 2019).

Based on these two techniques of capacitive and FPI, the pressure is sensed by the means of capacitance and deflection respectively. As far as the sensing physics is concerned, the capacitance sensor computes capacitance between electrodes by surface integration of local capacitance, and the optical sensor senses the gap at a local point of the central portion within a micro-domain. Hence, the capacitance sensor takes care of the diaphragm deflection on the entire surface which includes the diaphragm deflection in global form. However, optical does not. But these two sensors work by sensing the diaphragm deflection only. In short, the diaphragm deflection is the key to designing the sensor's performance in terms of sensitivity and accuracy (Catling 1998; Perić et al. 2018; Jena et al. 2021).

Nowadays, technology demands to miniaturize everything which also requires micro-scale sensors and this is how micro-electromechanical systems (MEMS) and nanoelectromechanical systems (NEMS) are taking shape for technology development (Lou et al. 2011; Xu et al. 2021). Thus, the manufacture of more sensitive sensors plays a significant role in miniature sensors to cater to the demand for pressure measurement on a micro-scale (Wilson et al. 2007). When the diaphragm miniaturization comes into the picture, it needs to reduce its diameter which further reduces the deflection sensitivity exponentially. To overcome this issue of sensitivity, the designer needs to reduce the thickness of the diaphragm and the reduction in the thickness needs one more order higher to diameter as the diaphragm deflection is proportional to 4th order polynomial of diameter and inverse proportional to the 3rd order polynomial of thickness (Jena et al. 2021; Bao 2000). It means that the proportion of reduction in diameter and thickness shall not be the same. Although, the diaphragm demands more reduction in thickness and this introduces the size effect on the diaphragm deflection which changes the characteristics of the diaphragm deflection (Li et al. 2018).

Given this, miniaturization of the sensing diaphragm is one of the challenging attributes for the diaphragm design to match with actual or experimental results (Jiranusornkul et al. 2020). In general, the diaphragm deflection behaviors become non-linear or highly non-linear as the conventional elasticity theory of bending does not predict the deflection due to strain gradient. In these conditions, the effect of the strain gradient phenomenon starts dominating. In the last decade, little work has been carried out to develop a mathematical model to include the strain gradient phenomena into the diaphragm deflection with few assumptions. However, these models also consist of some errors as they are simplified with the help of a few assumptions for avoiding higher-order on non-linearity terms, and their applicability to design thin diaphragm is not accurate. Hence, a modified strain gradient elasticity theory considering the size effect was developed by (Lam et al. 2003). This study reveals the size effect at various levels of Poisson ratio on the bending rigidity and they found that a non-dimensional bending rigidity due to strain gradient reduces with an increase in thickness or Poisson ratio. The strain gradient also affects a small amount of nonlinearity on the deflection with respect to the applied load. However, this theory does not account for the effect of operating pressure range on the bending rigidity. (Ma et al. 2012) have reported that the deflection of the diaphragm is highly non-linear to the applied pressure when the thickness is on a nanometric scale. While comparing the deflection behavior with pressure, it is clear that the thin diaphragm results in non-linearity. When the thickness is further reduced up to nanometric scale, applied pressure introduces non-linearity as shown in the experimental results (Ma et al. 2012). This study indicates that there could be a strong influence of pressure on the strain gradient. (Akgöz and Civalek 2015) had implemented Navier solution procedure to derive analytical solutions for deflection of beam to study the size-effect. In this, a new size-dependent beam theory was developed by using hyperbolic shear deformation beam and modified strain gradient theory considering the minimum total potential energy principle. A higher-order equation is solved based on the strain gradient elasticity theory through Hamilton's principle for the equation of motion of a micro-scaled bar to investigate the effects of the length scale parameters on natural frequencies of the bar (Akgöz and Civalek 2014). This work found that the size effect is more significant when the ratio of the micro-bar diameter to the length scale parameter is small. Furthermore, higher-order shear deformation micro-beam models in conjunction with modified strain gradient theory is used to study the bending response of single-walled carbon nanotubes (SWCNTs) embedded in an elastic medium (Akgöz and Civalek 2016). For this study, analytical method was proposed through the Navier-type solution for the simply supported embedded SWCNTs. This study shows that the bending behavior of SWCNTs is dependent on the small-size with slenderness ratio and stiffness of the elastic foundation. Another work was carried out for the bending analysis on single-walled carbon nanotubes (CNT) based on modified couple stress and strain gradient elasticity theories and Euler–Bernoulli beam theory. The size effect is taken into consideration using the modified couple stress and strain gradient elasticity theories. This work shows the significant effect of small-scale on the bending of CNT (AkgÖz and Civalek 2012). (Van Hieu et al. 2022) have developed a model of an electrostatic functionally graded (FG) micro-actuator based on the

nonlocal strain gradient theory (NSGT) incorporated the thickness effect and the Euler–Bernoulli beam theory (EBT) with the von-Karman's assumption for micro-beam application. They proposed an analytical solution which is solved by applying Galerkin and He's Laplace methods. In the same view, (Thai et al. 2017) have reviewed on the development of higher-order continuum models for the size effects in micro- and nano-structures such as beam, plate and shell using the nonlocal elasticity theory, modified couple stress theory and strain gradient theory. They have discussed higher-order continuum theory for the size-effect based on the classical theory, first-order shear deformation theory and higher-order shear deformation theory. The review indicates that the amount of work in the field of finite element analysis is relatively less compared with the analytical work. Moreover, analytical methods are limited to beam and plate structures only.

Based on the literature, the diaphragm bending rigidity behavior gets affected in a non-linear fashion due to the variation in size or thickness of the diaphragm and applied pressure. To date, the literature does not show a fundamental mechanism of inducing strain gradient due to the size effect on the diaphragm. Thus, there is a need to study the size effect and the mechanism of 'strain gradient' in depth so that the diaphragm can be accurately designed and optimized for its superior performance.

Hence, a set of finite element analysis is carried out to investigate the mechanism of the strain gradient due to the size effect and the same is discussed in the following sections.

2 Modeling for finite element analysis

In this paper, a circular diaphragm is selected for a wide range of pressure (0 to 1000 mbar) so that it can be suitable for both pressures as well as vacuum sensing. To investigate the size effect on the diaphragm deflection characteristics, the FEA model is constructed in COMSOL multi-physics software as shown in Fig. 1a, b. Where, 'Un' is displacement along normal direction, 'u' is the displacement along the x-direction, 'v' is the displacement along the y-direction, 'w' is the displacement along the z-direction, 'ur' is the displacement along the radial direction, and 'nx, ny and nz' indicate normal unit vector along x, y, and z-direction respectively.

Figure 1a shows a model in 2-dimensional axisymmetric geometry to reduce the computation time significantly. However, this model may not include the effect of strain gradient due to circumferential stretching stress and bending moment. In view of this, a 3-dimensional model is also constructed to understand the effect due to the pressure-induced circumferential stretching as shown in Fig. 1b. Figure 1a, b also show boundary conditions of displacement components of (u, v, w) which is used to allow the mesh deformation of the diaphragm.

Governing equation for FEA simulation in COMSOL is derived from force equilibrium as presented in Eq. 1. In general, this equation is being solved to predict the deflection and stress on the diaphragm without deforming or changing cross-sections and their orientation to the axis of the diaphragm. This geometric condition with Eq. 1 leads to another derived differential equation of a beam along the X-axis as presented in Eq. 2 which is also derived from the Euler–Bernoulli theory (Öchsner 2021). Equation 2 is further simplified for a circular diaphragm and presented in Eq. 3.

$$\nabla \cdot \sigma + \mathrm{Fv} = 0 \tag{1}$$

where 'σ' is stress and Fv is the volume force in the structure respectively.

$$\frac{d^2}{dx^2}\left(\mathrm{EI}\frac{d^2w}{dx^2}\right) + C_f = q \tag{2}$$

where 'E' is the modulus of elasticity, 'I' is the second moment of inertia, 'w' is deflection, 'C_f' is the elastic foundation modulus and 'q' is the distributed transverse load.

$$D_o\nabla^4 w = q$$

$$D_o = \frac{Et^3}{12(1-\nu^2)} \tag{3}$$

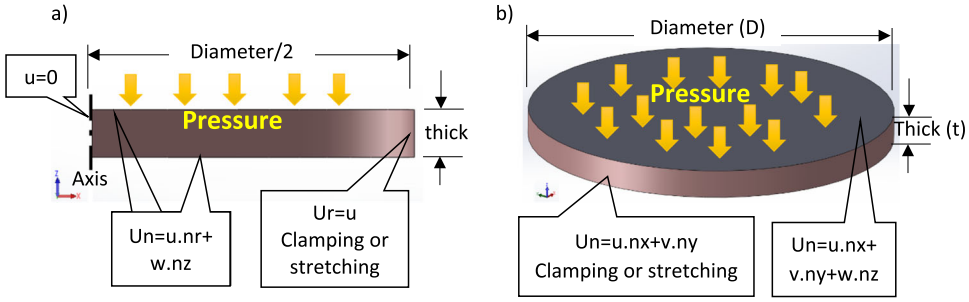

Fig. 1 Model of FEA simulation. **a** Two-dimensional axisymmetric model. **b** Three-dimensional model

where 't' is the thickness, 'v' is the poison's ratio and 'D_O' is the bending rigidity or flexural rigidity of the diaphragm (Landau and Lifshitz 1986).

The Eqs. (1–3) do not account for the strain gradient effect on the diaphragm. To incorporate the strain gradient effect or other possibilities of physics due to the size effect, it is essential to deform the geometry of the diaphragm as per the computed value of the displacement components of the diaphragm deflection. This is possible by allowing the mesh deformation during FEA simulation simultaneously. The effect of mesh deformation needs to be fully coupled with the FEA computed deformation parameters and the same is presented in Fig. 2 for better clarity.

Initially, the displacement (u, v, w) in all directions (x, y, z) are computed as per the governing Eq. 1, and the boundary conditions like applied pressure and clamping condition shown in Fig. 1a, b. These displacements are further used to deform or move the mesh of the diaphragm. After the mesh deformation, resisting forces, tractions or stresses induces bending moment (M1 and M2) to resist the diaphragm displacement. This effect tries to reverse the diaphragm displacement which is recalculated after mesh deformation due to M1and M2. If the error or change in the deflection due to the mesh deformation (by 1step size of the iteration) is not less than 0.1%, FEA calculation works on an iterative loop until the error gets settled below 0.1%. If it is also not getting reduced below0.1%, the solver reduces

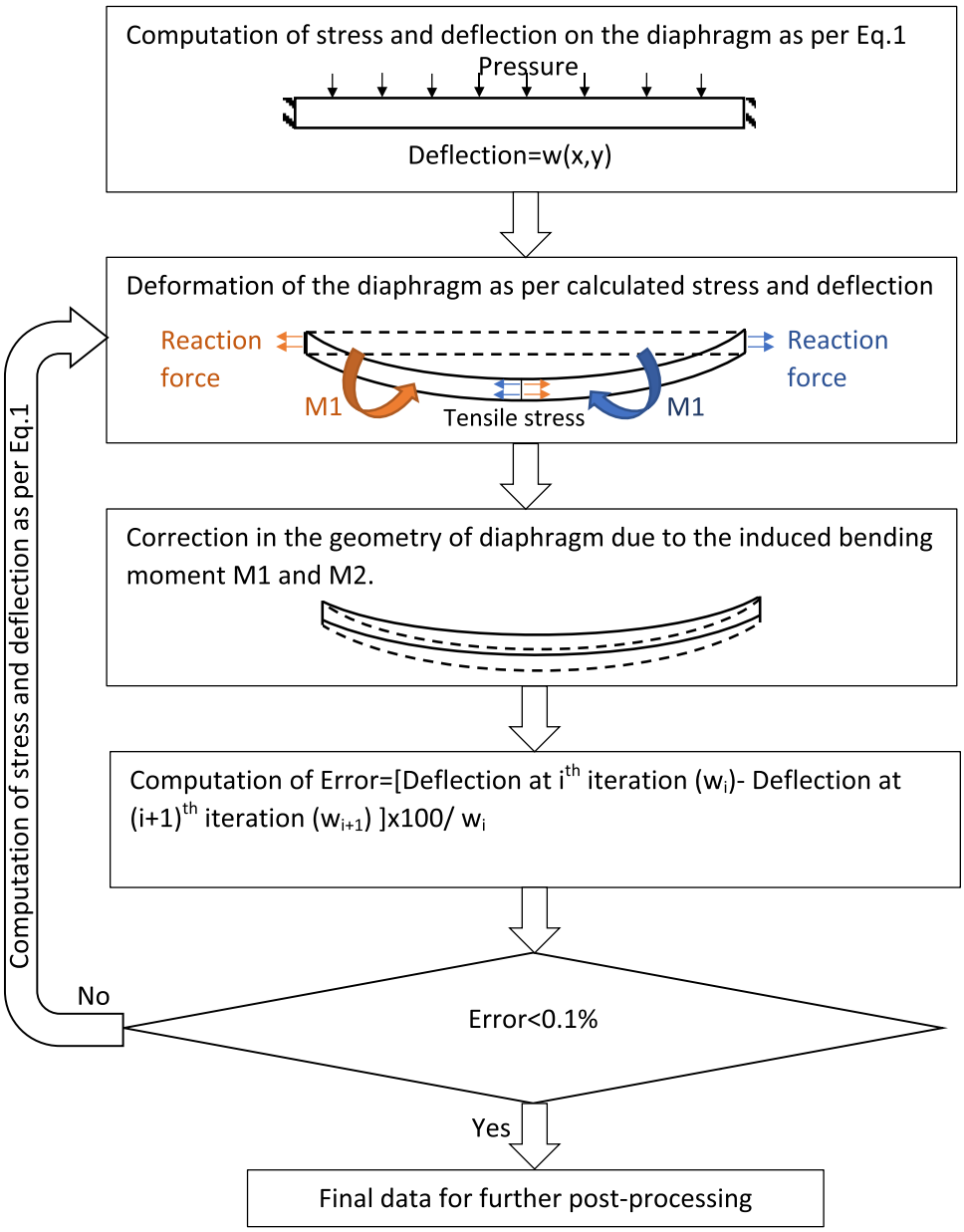

Fig. 2 Flow diagram to implement moving-mesh to study the strain gradient effect on the diaphragm. The dotted line indicates the geometry before geometry or mesh deformation

the iterative step size automatically to converge the solution. Thus, full coupling of solid mechanics and mesh deformation is implemented as per the flow diagram of Fig. 2 in COMSOL 5.5. The relevant parameters for the FEA simulation are listed in Table 1. In this table, length scale parameter is used to define the diaphragm thickness from the non-dimensional value of the thickness ratio 'n' to identify thinner and thicker diaphragm. Where, the diaphragm thickness equals to the length scale multiplication to the thickness ratio. Hence, higher value of 'n' indicates thicker diaphragm and lesser value indicates thinner diaphragm.

As far as meshing is concerned, it plays a critical role in the accuracy of the computed data as FEA is an approximation method whose quality of results depends on mesh size. In general, the solution of FEA would be ideal if mesh size is infinitesimally small. However, a smaller mesh size leads to an increase in the computation efforts and requires prolonged computation time. Because of this, a set of simulations is carried out to evaluate convergency on the deflection of the diaphragm and the computation time for three different thicknesses of 0.5 μm, 1.0 μm, and 1.5 μm as shown in Fig. 3a–c.

Figure 3a–c shows that the change in convergencies due to the mesh size is 65%, 14%, and 03% for the diaphragm thickness of 0.5 μm, 1.0 μm, and 1.5 μm respectively.

In the case of a thin diaphragm, the change in the convergency reduces drastically when the mesh size increases. This result indicates that the phenomenon of the strain gradient makes this model highly non-linear, and due to this, the solver for the FEA model is set to highly non-linear (Newton) (Lampron et al. 2021). Here, the analysis shows that the effect of mesh size is very sensitive to the diaphragm diameter to thickness ratio. For example, the diaphragm diameter to thickness ratio of more than 1000 requires mesh optimization. Thus, the designer has to consider mesh optimization when they are modeling any structure whose 'diameter to thickness' ratio is more than 1000 or aspect ratio (t/D) of any feature is less than 0.001.

Thus, the optimum mesh size is an important parameter to investigate the size effect accurately. Hence, the mesh size is optimized for convergence accuracy better than 95% with reasonably low computation time, which are suitable for the present work as shown in Fig. 3a. The optimized mesh size of [maximum size = 0.1 mm and minimum size = 0.01 mm] takes 85 s to solve FEA model in Intel(R) Core™ i3-9100F CPU @ 3.60 GHz processor.

3 Results and discussion

As per the classical bending theory of a diaphragm or a beam, radial stress and strain become higher on the surface and it reduces while moving towards mid-plane. Where the mid-plane exists at the middle of thickness, i.e., at 'Z' equal to half of the thickness. To investigate the theory of strain gradient by the size effect, radial strain along the mid-plane is calculated at an applied pressure of 100 Pa and mapped for the thickness ratio from1 to 7 as presented in Fig. 4a, b. Figure 4a shows the radial strain at the mid-plane for the 2D axisymmetric model and Fig. 5b is plotted for the 3D model. The magnitude of strain is of the order of 10^{-4} which is very small but they are non-zero. It is seen that both models show the same amount of strain for all ranges of thickness. The magnitude of strain is significantly depending on the thickness. In the case of a thinner diaphragm (thickness ratio = 1), strain is much higher. On other hand, the strain reaches zero as the thickness increases. The strain along the radial position is also not uniform. It shows a combination of linear and quadratic decrement which will cause to induce bending moment to change the deflection shape and size of the diaphragm to the classical theory of bending. Because of this, strain gradient along the radial direction is computed and plotted in Fig. 5a, b.

Figure 5a shows radial strain gradient for the 2D-axisymmetric model at various levels of thickness. The strain gradient is zero at the center of the diaphragm as the diaphragm shape gets retained at the center due to the axisymmetric geometric and boundary condition of the model. The result also shows that the maximum value of the strain gradient shifts radially outward with the decrement of the thickness. This indicates that the induced bending moment on the diaphragm is higher at the periphery when the diaphragm is sufficiently thin. The thin diaphragm has a low moment of inertia against bending which helps to deflect the diaphragm easily near the central portion without inducing strain gradient and this is how the gradient significantly appears near the periphery. On other hand, the thick diaphragm comparatively exhibits a high moment of inertia which helps to shift the maximum strain gradient near the central portion. The amplitude of strain gradient is less in the case of a thick diaphragm which is due to the relatively high stiffness of the thick diaphragm which resists deflection.

Figure 5b shows radial strain gradient for a 3D model which also shows the same behavior and same amplitude. It means that both models are similar as far as strain gradient is concerned. However, few deviations near the center and periphery are observed when Fig. 5a is compared with Fig. 5b. Thus, bending rigidity is also analyzed for both

Table 1 Parameters for FEA simulation

Sr. No.	Parameters	Value	Remark
1	Pressure	0-1000 Pa	Study parameters
2	Stretching stress	0 MPa	
3	Diameter	1 mm	
4	Length scale	0.5 µm	Geometric parameters
5	Thickness ratio (n)	2-7	
6	Thickness	nx0.5 µm	
7	Material (Silicon, single-crystal, isotropic)	Density: 2329 kg/m^3, Modulus of elasticity: 170 GPa, Poisson's ratio: 0.28	Materials parameters
8	Mesh deformation	Mesh smoothing type: hyperelastic	FEA solver details
9	Type of study	Stationary (steady-state)	
10	Relative tolerance	0.001	
11	Linearity	Nonlinear: Highly nonlinear (Newton)	
12	Solver	PARDISO	
13	Pivoting perturbation	10^{-9}	

models as the strain gradient affects the bending behavior of the diaphragm due to the deflection-induced bending moment on the diaphragm to suppress the deflection.

Hence, bending rigidity is computed and plotted in Fig. 6a, b. The bending rigidity increases exponentially with the diaphragm thickness. This can be explained by Eq. 3 where the bending rigidity is proportional to the 3rd order polynomial of the thickness as per the classical bending theory. The results also show that the applied pressure increases it linearly and it is insignificant in the case of the thick diaphragm. It is due to the development of strain gradient over a large area of the diaphragm. The thinner diaphragm results in an increased zone of influence for the strain gradient as shown in Fig. 5a, b, which leads to highly non-linear deflection with pressure. Thus, the bending rigidity is getting affected significantly on the thin diaphragm due to the change in pressure. Hence, modeling of a diaphragm with conventional theory yields erroneous results (Li et al. 2018; Lam et al. 2003).

Figure 6a shows bending rigidity for the 2D-axisymmetric model and Fig. 6b shows the same for the 3D model. Both exemplify the same trend and magnitude of bending rigidity. This result does not show any significant changes between these two models. Hence, the ratio of bending rigidity for both models are further computed and plotted for various level of pressure and thickness as presented in Fig. 7. It is seen that the effect of pressure is within 1.2% (i.e., from 0.994 to 1.008). This small variation might be happening due to the variation in the mesh of the 3D model to 2D. Thus, both models yield similar results provided the 3D model's mesh is optimized as per Fig. 1. Hence, the 2D model can be used if the model is axisymmetric (geometry and boundary conditions) as it takes a very low time of computation. In other cases, a non-symmetric, 3D model with optimized mesh needs to be selected.

The analysis study till now is not very clear about the effect of size on the bending rigidity. Hence, it is essential to compare the bending rigidity due to the effect of strain gradient to the classical bending theory. Therefore, a parameter called non-dimensional bending rigidity (Lam et al. 2003) is computed and studied further for the thickness as well as pressure. Here, the non-dimensional bending rigidity is the ratio of bending rigidity with 'moving-mesh' and without moving-mesh, where, moving-mesh implies in the bending rigidity with strain gradient and without moving-mesh belongs to the classical bending theory.

Hence, bending rigidity with moving-mesh (for strain gradient) and without moving-mesh are evaluated and their ratio is plotted in Fig. 8. It is observed that the magnitude of the non-dimensional bending rigidity is more for the thin diaphragm (n = 1). It is also found that the thicker diaphragm tries to converge at 1 which means that higher thickness does not have any effect on the strain gradient. This increase in non-dimensional bending rigidity at the low thickness and higher pressure is happening due to a large strain gradient which further induces a large resisting

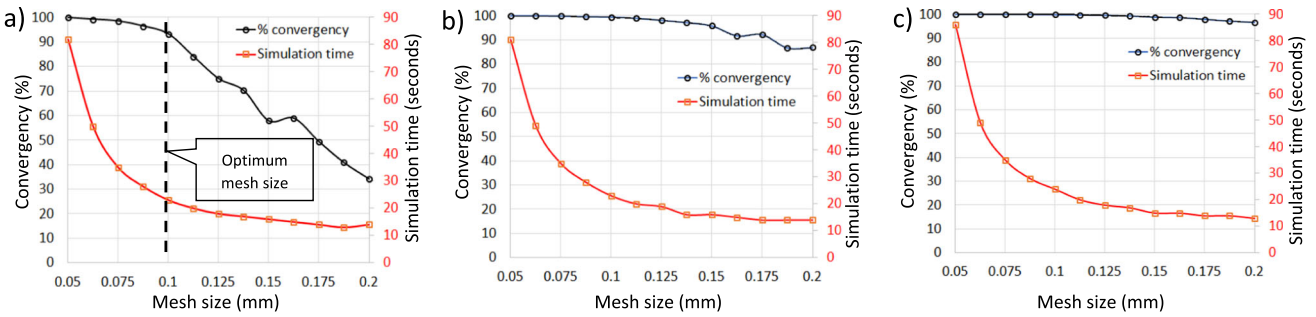

Fig. 3 Mesh optimization for convergency of FEA result to the analytical solution. **a** With the diaphragm thickness = 0.5 µm, **b** diaphragm thickness = 1.0 µm and **c** diaphragm thickness = 1.5 µm

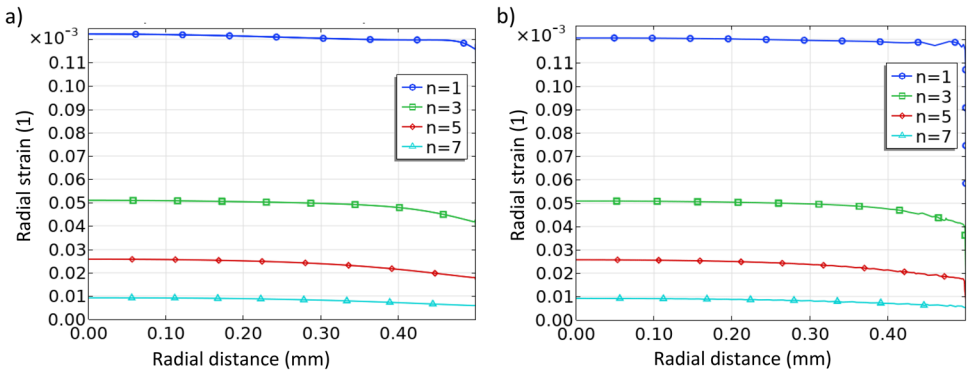

Fig. 4 Radial strain at z = thickness/2 to measure the strain along the mid-plane. **a** In the case of the 2D axisymmetric model. **b** In the case of the 3D model

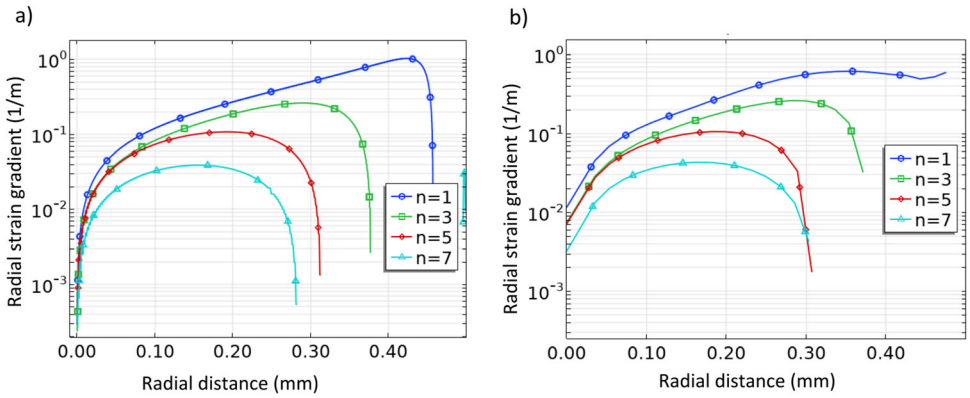

Fig. 5 Radial strain gradient along the mid-plane, at z = thickness/2. **a** For the 2D axisymmetric model. **b** For 3D model

bending moment (M1 and M2 as shown in Fig. 2). Thus, the diaphragm deflects less than the classical theory, and the modified bending rigidity (Li et al. 2018) increases. This increment in the rigidity significantly depends on the diaphragm thickness and it also depends on applied pressure up to some extent which was not addressed so far. Hence, the sensor's diaphragm designers need to address the modified bending rigidity for both attributes of thickness as well applied pressure.

3.1 Comparison with literature

The non-dimensional bending rigidity is compared with the theoretical values from the literature (Li et al. 2018; Lam et al. 2003) and compared with the present FEA model at 100 Pa and 1000 Pa. Figure 9a, b show the literature values are lying within the band of 100 to 1000 Pa of pressure level for a wide range of thickness. Moreover, the trend of the bending rigidity shows a good agreement. In the case of a lower thickness (i.e., at n = 1–4), the bending rigidity of literature is tending towards 100 Pa as the theoretical model ignores the effect of pressure at higher-order and which reduces the bending rigidity to the actual value. In the case of the thick diaphragm (n = 4–7), the bending rigidity moves towards 1000 Pa, this is due to the effect of a linear relation of deflection with pressure which dominates at classical bending theory of large thickness. In short, n = 1–4, the effect of thickness dominates which

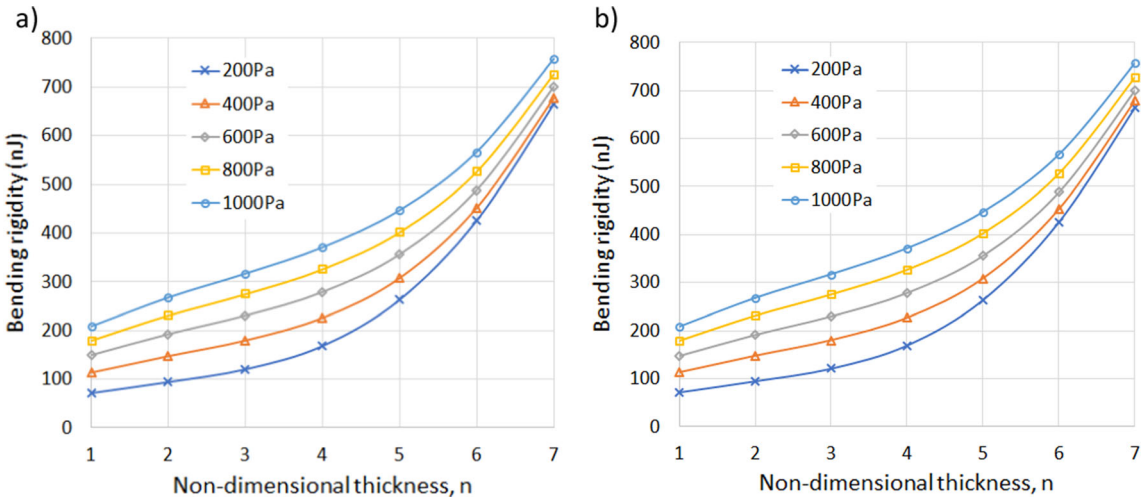

Fig. 6 Bending rigidity vs thickness with various levels of pressure. **a** For a 2D axisymmetric model. **b** For 3D model

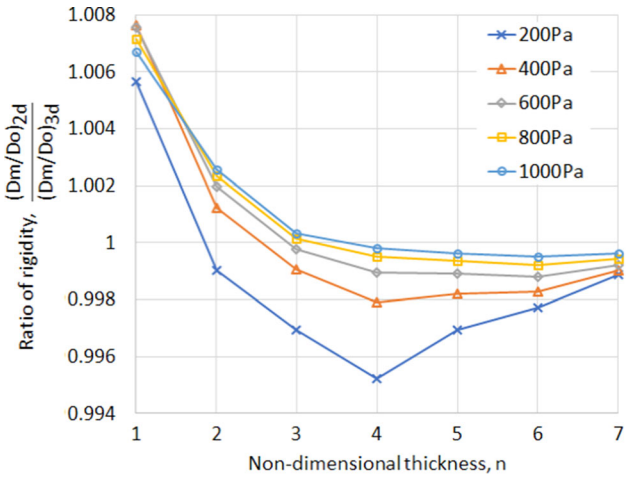

Fig. 7 Ratio of bending rigidity Vs thickness with various levels of pressure to compare for the 2D axisymmetric model and the 3D model

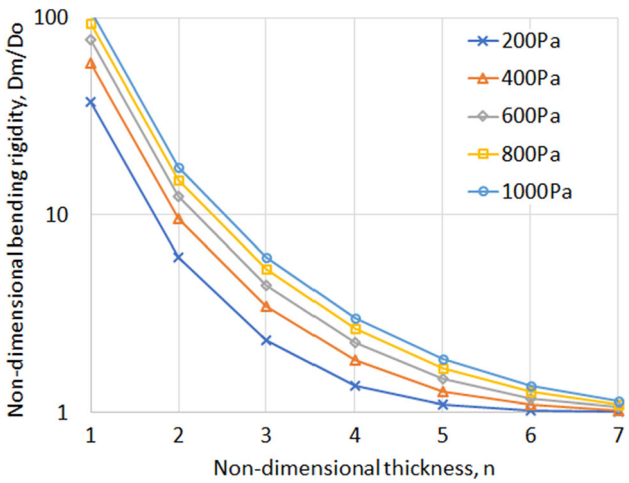

Fig. 8 Non-dimensional bending rigidity vs thickness with various levels of pressure

allows more rigidity with pressure. Moreover, at n = 4–7, the effect of pressure dominates and the actual rigidity reduces and tries to approach near to the classical bending theory.

To further validation about the diaphragm deflection with experimental results, the FEA model is modified as per the literature model in 3D form of literature (Jiranusornkul et al. 2020). The results of the FEA model are compared with experimental results of literature (Jiranusornkul et al. 2020) for benchmarking of the present FEA method as shown in Table 2 and also presented in Fig. 10. The maximum deviation of the present model from the literature data is within 20 microns and accuracy is less than 1%. It shows a non-linear behavior of the deflection, but a good agreement between the proposed model with experimental result. This supports the accuracy and correctness of the FEA model presented in this paper. Thus, the presented FEA model has the potential to model, optimize and predict diaphragm behavior for pressure sensors or actuators more accurately.

Moreover, the presented FEA modeling method has the capability to evaluate or study the following attributes of the diaphragm design more accurately such as 'effect of thickness and pressure on linearity', 'improvement of linearity due to stretching (radial stretching of the diaphragm)' and 'improvement of linearity due to introducing island or micro-features'.

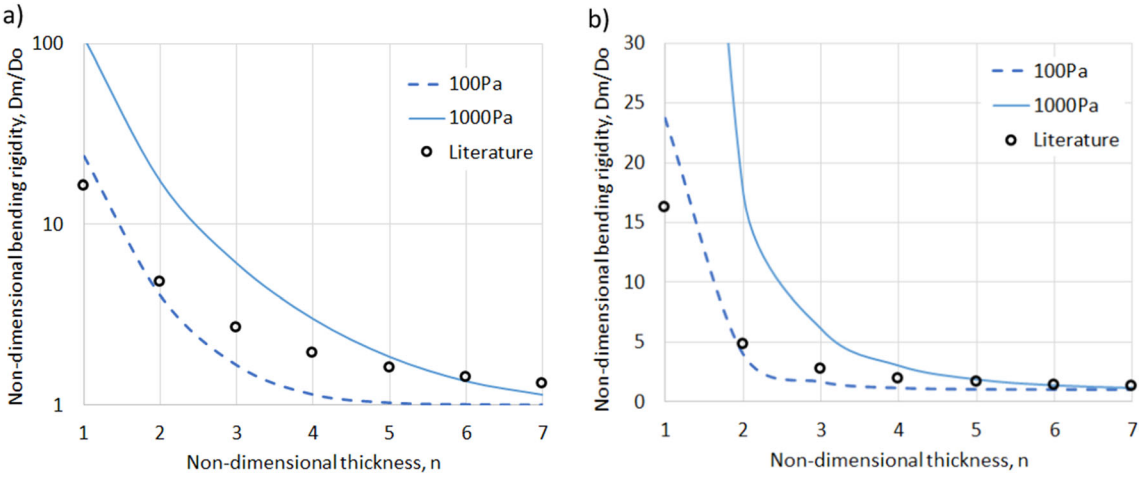

Fig. 9 Comparison of non-dimensional bending rigidity with the strain gradient theory. **a** The plot in logarithmic scale. **b** The plot in linear scale

Table 2 Benchmarking table for FEA simulation wit respect to the literature value

Sr. no.	Pressure (kPa)	Deflection (mm)		Deviation (μm)
		Experimental (Jiranusornkul et al. 2020)	Simulation	
1.	1.72	0.067	0.059	8
2.	3.49	0.118	0.115	3
3.	5.21	0.163	0.165	− 2
4.	6.98	0.198	0.211	− 13
5.	8.66	0.239	0.251	− 12
6.	10.47	0.284	0.292	− 8
7.	12.24	0.326	0.331	− 5
8.	13.92	0.377	0.368	9
9.	15.64	0.418	0.402	16
10.	17.37	0.444	0.435	9

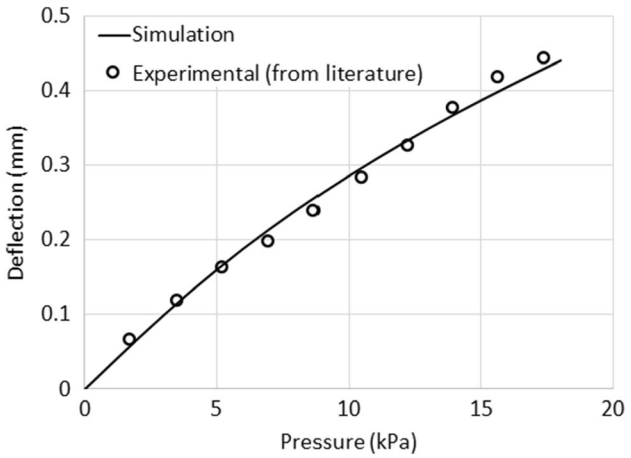

Fig. 10 Validation of FEA simulation with experimental results taken from literature

4 Conclusion

In the present work, a diaphragm for a pressure sensor is modeled and simulated to investigate the effect of strain gradient on bending rigidity and deflection characteristics. Based on the modeling and simulation work, the following are the main conclusions drawn.

- Mesh size significantly introduces convergency error for an FEA model to investigate the phenomenon of the strain gradient. The convergency error starts dominating when the aspect ratio of the diaphragm is less than 0.001 and it makes the model highly non-linear.
- To design and optimize the diaphragm for micro-scale sensors through FEA modeling, a highly non-linear (Newton) solver with optimized mesh is essentially required.
- The strain gradient is zero at the center and periphery, and maximum on other portions which leads to induce resisting bending-moment to increase actual or

modified bending rigidity. The extent of strain gradient spreads on the diaphragm due to low thickness as well as high pressure.

- The bending rigidity depends on thickness as well as pressure. The bending rigidity keeps changing for all ranges of applied pressure when a specific thickness is selected.
- In the case of a thinner diaphragm (aspect ratio $<$ 0.001), the effect of thickness dominates which allows more rigidity with pressure. On other hand, the effect of pressure dominates for higher thickness (aspect ratio $>$ 0.001) and the actual rigidity reduces which tries to approach near to the classical bending theory.
- Diaphragm deflection shows non-linear behavior with applied pressure and the same is experimentally validated with literature and they found a good agreement.
- The presented method of finite element analysis can model sensors at a micro-scale as well as meso-scale more accurately to improve the linearity, sensitivity, and accuracy of a pressure sensor.

References

AkgÖz B, Civalek Ö (2012) Investigation of size effects on static response of single-walled carbon nanotubes based on strain gradient elasticity. Int J Comput Methods. https://doi.org/10.1142/S0219876212400324

Akgöz B, Civalek Ö (2014) Longitudinal vibration analysis for microbars based on strain gradient elasticity theory. Jvc/journal Vib Control. https://doi.org/10.1177/1077546312463752

Akgöz B, Civalek Ö (2015) A novel microstructure-dependent shear deformable beam model. Int J Mech Sci. https://doi.org/10.1016/j.ijmecsci.2015.05.003

Akgöz B, Civalek Ö (2016) Bending analysis of embedded carbon nanotubes resting on an elastic foundation using strain gradient theory. Acta Astronaut. https://doi.org/10.1016/j.actaastro.2015.10.021

Bao MH (2000) Chapter 2 Basic mechanics of beam and diaphragm structures. Handbook sensors actuators. Elsevier, Amsterdam. https://doi.org/10.1016/S1386-2766(00)80016-X

Catling DC (1998) High-sensitivity silicon capacitive sensors for measuring medium-vacuum gas pressures. Sens Actuators A Phys 64:157–164. https://doi.org/10.1016/S0924-4247(98)80009-5

Chen L, Mehregany M (2008) A silicon carbide capacitive pressure sensor for in-cylinder pressure measurement. Sensors Actuators A Phys. https://doi.org/10.1016/j.sna.2007.09.015

Eswaran P, Malarvizhi S (2013) MEMS capacitive pressure sensors: a review on recent development and prospective. Int J Eng Technol 5:2734–2746

Gabrielson TB (1993) Mechanical-thermal noise in micromachined acoustic and vibration sensors. IEEE Trans Electron Devices. https://doi.org/10.1109/16.210197

Ghildiyal S, Ranjan P, Mishra S, Balasubramaniam R, John J (2019) Fabry-Perot interferometer-based absolute pressure sensor with stainless steel diaphragm. IEEE Sens J. https://doi.org/10.1109/JSEN.2019.2909097

He Z, Chen W, Liang B, Liu C, Yang L, Lu D et al (2018) Capacitive pressure sensor with high sensitivity and fast response to dynamic interaction based on graphene and porous nylon networks. ACS Appl Mater Interfaces. https://doi.org/10.1021/acsami.8b01050

Hu J, Duan W, Fan S, Xiao H (2022) A triangular wavy substrate-integrated wearable and flexible piezoelectric sensor for a linear pressure measurement and application in human health monitoring. Measurement 190:110724. https://doi.org/10.1016/J.MEASUREMENT.2022.110724

Jena S, Pandey C, Gupta A (2021) Mathematical modeling of different diaphragm geometries in MEMS pressure sensor. Mater Today Proc. https://doi.org/10.1016/j.matpr.2020.11.249

Jiang J, Zhang T, Wang S, Liu K, Li C, Zhao Z et al (2017) Noncontact ultrasonic detection in low-pressure carbon dioxide medium using high sensitivity fiber-optic Fabry-Perot sensor system. J Light Technol. https://doi.org/10.1109/JLT.2017.2765693

Jiranusornkul N, Kraduangdej S, Niltawach N, Pimpin A, Srituravanich W (2020) Development of a paper-based pressure sensor fabricated by an inkjet-printed water mask method. Microsyst Technol 26:2117–2121. https://doi.org/10.1007/s00542-020-04771-3

Kim Y, Neikirk DP (1995) Micromachined Fabry-Perot cavity pressure transducer. IEEE Photonics Technol Lett 7:1471–1473. https://doi.org/10.1109/68.477286

Lam DCC, Yang F, Chong ACM, Wang J, Tong P (2003) Experiments and theory in strain gradient elasticity. J Mech Phys Solids. https://doi.org/10.1016/S0022-5096(03)00053-X

Lampron O, Therriault D, Lévesque M (2021) An efficient and robust monolithic approach to phase-field quasi-static brittle fracture using a modified Newton method. Comput Methods Appl Mech Eng. https://doi.org/10.1016/j.cma.2021.114091

Landau LD, Lifshitz EM (1986) Theory of elasticity, Third Edition: (Course of Theoretical Physics), Pergamon Press, Oxford

Lee YS, Wise KD (1982) A batch-fabricated silicon capacitive pressure transducer with low temperature sensitivity. IEEE Trans Electron Devices. https://doi.org/10.1109/T-ED.1982.20656

Lei KF, Lee KF, Lee MY (2012) Development of a flexible PDMS capacitive pressure sensor for plantar pressure measurement. Microelectron Eng. https://doi.org/10.1016/j.mee.2012.06.005

Li G, Li D, Cheng Y, Sun W, Han X, Wang C (2018) Design of pressure-sensing diaphragm for MEMS capacitance diaphragm gauge considering size effect. AIP Adv. https://doi.org/10.1063/1.5021374

Li J, Jia P, Fang G, Wang J, Qian J, Ren Q et al (2022) Batch-producible all-silica fiber-optic Fabry-Perot pressure sensor for high-temperature applications up to 800 °C. Sens Actuators A Phys 334:113363. https://doi.org/10.1016/J.SNA.2022.113363

Lou L, Zhang S, Lim L, Park WT, Feng H, Kwong DL et al (2011) Characteristics of NEMS piezoresistive silicon nanowires pressure sensors with various diaphragm layers. Procedia Eng. https://doi.org/10.1016/j.proeng.2011.12.354

Ma J, Jin W, Ho HL, Dai JY (2012) High-sensitivity fiber-tip pressure sensor with graphene diaphragm. Opt Lett. https://doi.org/10.1364/ol.37.002493

Öchsner A (2021) Euler-Bernoulli beam theory. Class Beam Theor Struct Mech. https://doi.org/10.1007/978-3-030-76035-9_2

Perić B, Simonović A, Ivanov T, Stupar S, Vorkapić M, Peković O et al (2018) Design and testing characteristics of thin stainless steel diaphragms. Procedia Struct Integr. https://doi.org/10.1016/j.prostr.2018.12.141

Sanli H, Alptekin E, Canakci M (2022) Using low viscosity micro-emulsification fuels composed of waste frying oil-diesel fuel-higher bio-alcohols in a turbocharged-CRDI diesel engine. Fuel 308:121966. https://doi.org/10.1016/J.FUEL.2021.121966

Thai HT, Vo TP, Nguyen TK, Kim SE (2017) A review of continuum mechanics models for size-dependent analysis of beams and plates. Compos Struct. https://doi.org/10.1016/j.compstruct.2017.06.040

Van Hieu D, Chan DQ, Phi BG (2022) Analysis of nonlinear vibration and instability of electrostatic functionally graded micro-actuator based on nonlocal strain gradient theory considering thickness effect. Microsyst Technol. https://doi.org/10.1007/s00542-022-05321-9

Wan S, Bi H, Zhou Y, Xie X, Su S, Yin K et al (2017) Graphene oxide as high-performance dielectric materials for capacitive pressure sensors. Carbon N Y. https://doi.org/10.1016/j.carbon.2016.12.023

Wang H, Tao J, Jin K, Wang X, Dong Y (2022) Multifunctional pressure/temperature/bending sensor made of carbon fibre-multiwall carbon nanotubes for artificial electronic application. Compos Part A Appl Sci Manuf 154:106796. https://doi.org/10.1016/J.COMPOSITESA.2021.106796

Wilson SA, Jourdain RPJ, Zhang Q, Dorey RA, Bowen CR, Willander M et al (2007) New materials for micro-scale sensors and actuators. An engineering review. Mater Sci Eng R Rep. https://doi.org/10.1016/j.mser.2007.03.001

Xu M, Feng Y, Han X, Ke X, Li G, Zeng Y et al (2021) Design and fabrication of an absolute pressure MEMS capacitance vacuum sensor based on silicon bonding technology. Vacuum. https://doi.org/10.1016/j.vacuum.2021.110065

Yin J, Liu T, Jiang J, Liu K, Wang S, Qin Z et al (2014) Batch-producible fiber-optic fabry-pérot sensor for simultaneous pressure and temperature sensing. IEEE Photonics Technol Lett. https://doi.org/10.1109/LPT.2014.2347055

Young DJ, Du J, Zorman CA, Ko WH (2004) High-temperature single-crystal 3C-SiC capacitive pressure sensor. IEEE Sens J. https://doi.org/10.1109/JSEN.2004.830301

Zhou MX, Huang QA, Qin M, Zhou W (2005) A novel capacitive pressure sensor based on sandwich structures. J Microelectromech Syst. https://doi.org/10.1109/JMEMS.2005.859100